Electronic Journal of Biotechnology 60 (2022) 26–35

Contents lists available at ScienceDirect

Electronic Journal of Biotechnology

journal homepage: www.elsevier.com/locate/ejbt

Research Article

Biogenesis of nanoparticles with inhibitory effects on aflatoxin B_1 production by *Aspergillus flavus* ☆

Huda Sheikh [a,b,*], Mohamed F. Awad [c,d]

[a] Department of Biological Science, Faculty of Science and Arts, King Abdulaziz University, Rabigh Campus, P.O. Box 344, 21911 Rabigh, Saudi Arabia
[b] Department of Biology, College of Science, University of Jeddah, P.O. Box 80327, Jeddah 21589, Saudi Arabia
[c] Department of Biology, College of Science, Taif University, P.O. Box 11099, Taif 21944, Saudi Arabia
[d] Department of Botany and Microbiology, Faculty of Science, Al-Azhar University, Assiut 71524, Egypt

GRAPHICAL ABSTRACT

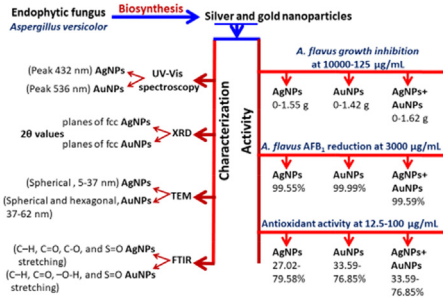

ARTICLE INFO

Article history:
Received 11 April 2022
Accepted 12 September 2022
Available online 16 September 2022

Keywords:
Aflatoxin B1
Antiaflatoxigenic
Aspergillus flavus
Fungal nanofactories
Gold nanoparticles
Green chemistry
Mycosynthesis
Silver nanoparticles

ABSTRACT

Background: Fungal nanofactories have been utilized to synthesize silver and gold nanoparticles. This study was designed to mycosynthesize and characterize silver and gold nanoparticles (AgNPs and AuNPs) and to study their effect on aflatoxin B_1 production by *Aspergillus flavus*.
Results: Silver and gold nanoparticles were synthesized by endophytic *Aspergillus versicolor* and then analyzed by UV–vis spectroscopy. The results revealed surface plasmon resonance peaks at 432 and 536 nm for Ag and Au nanoparticles, respectively. The obtained transmission electron microscopy results revealed the fashioning of spherical AgNPs and spherical and hexagonal AuNPs with a mean particle magnitude of 5–37 and 37–62 nm, respectively. X-ray diffraction showed the typical face-centered cubic structure of the mycosynthesized Ag and Au nanoparticles. An *in vitro* investigation showed that AgNPs, AuNPs, and their mixture at different concentrations (10000, 5000, 3000, 1000, 750, 500, 250, and 125 µg/mL) could inhibit or reduce the outgrowth and production of aflatoxin B_1 (AFB_1) by *A. flavus*. The concentration that showed no AFB_1 production was less than those for the inhibition of fungal growth. AgNPs, AuNPs, and their mixture also exhibited promising antiradical scavenging activity.
Conclusions: The use of fungi in the metallic nanoparticle's fabrication and the utilization of mycosynthesized nanoparticles is promising as a substitute of chemicals to control antiaflatoxigenic fungi.

Abbreviations: AFB_1, aflatoxin B_1; AgNPs, silver nanoparticles; AuNPs, gold nanoparticles; BHT, butylated hydroxytoluene; DPPH, 1,1-Diphenyl-2-picryl-hydrazyl; FTIR, Fourier Transform Infrared Spectroscopy; HPLC, high performance liquid chromatography; ITS, Internal Transcribed Spacer; PDA, potato dextrose agar; TEM, Transmission Electron Microscopy; TLC, thin-layer chromatography; XRD, X-ray diffraction; YES, yeast extract sucrose.

Peer review under responsibility of Pontificia Universidad Católica de Valparaíso.

* Corresponding author.
E-mail address: hmsheikh@kau.edu.sa (H. Sheikh).

https://doi.org/10.1016/j.ejbt.2022.09.003

How to cite: Sheikh H, Awad MF. Biogenesis of nanoparticles with inhibitory effects on aflatoxin B1 production by *Aspergillus flavus*. Electron J Biotechnol 2022;60. https://doi.org/10.1016/j.ejbt.2022.09.003.

1. Introduction

Nanoparticles, which are known to possess a dimension of 100 nm or less in size, [1] have gained growing awareness as inorganic antimicrobial agents in nonfood applications [2] because of their distinctive physical and chemical attributes, which vary considerably from their traditional coordinates [3]. Physical and chemical methods, which converge on utilizing a vast amount of chemicals and elevated temperature through radiation, are used to achieve the synthesis of metal nanoparticles. Modern investigations have shown the use of easy, neat, eco-friendly, inexpensive, and safe techniques for bio-fabrication of nanoparticles [4]. This involves the use of various biological resources that include bacterial, fungal, algal, plant, and animal metabolites to synthesize different metal nanoparticles [5,6,7,8,9]. Fungal nanofactories have been utilized to synthesize silver, platinum, silica, zirconium, iron titanium, and gold nanoparticles [1,10,11,12]. Green chemistry is a simple eco-friendly technique for the fabrication of metal nanoparticles in which fungi are employed for nanoparticle biosynthesis [13].

Aflatoxins are a small group of closely related heterocyclic secondary metabolites [14]. It was found as difuranocoumarin derivatives biosynthesized through a polyketide pathway [15]. Of the 20 well-characterized diverse sorts of aflatoxins, aflatoxins B_1, B_2, G_1, G_2, M_1, and M_2 are considered to be the most important ones [16], and along with aflatoxin B_1 (AFB_1), they are the most common and toxic toxins that cause a serious risk to human and animal health [17]. Aflatoxin B_1 is produced mainly by aflatoxigenic species of filamentous fungi, common saprophytes, and opportunistic pathogens *Aspergillus* (*A. flavus*, *A. parasiticus,* and *A. nomius*) [18]. Aflatoxin B_1 is the most common globally and reported in about 75 % of food and feeds contamination with aflatoxins [19,20].

Aflatoxin B_1, whose mutagenic, hepatic-carcinogenic, teratogenic, and immunosuppressive activity to a broad spectrum of living organisms has been widely studied [21], while the International Agency of Research on Cancer was classified AFB_1 as Group 1A carcinogen [22]. The European Commission has established 2 ng/g as the maximum level for AFB_1, 4 ng/g for combined aflatoxins in foodstuffs, and 0.05 ng/mL for AFM_1 in liquid milk [23]. Inhibiting the outgrowth of aflatoxigenic fungi is first necessary to prevent aflatoxins production in agricultural merchandises [24].

Physical, chemical, and biological methods to reduce aflatoxins can be employed for detoxification or removing from contaminated food and nutrients [25]. Larger surface area of nanoparticles, because of their size, interact with microorganisms rather than the larger shape of particles [26]. Thus, it may be functional to utilize nanoparticle-based modes as a substitutional remedy versus fungi [27]. The influence of silver nanoparticles on the development and AFB_1 biosynthesis of *Aspergillus parasiticus* was studied and determined in an earlier report [28]. This study aimed to evaluate antiaflatoxigenic activities using different concentrations of mycosynthesized AgNPs and AuNPs by *A. versicolor* individually/mixture on outgrowth and AFB_1 accumulation by *A. flavus*.

2. Materials and methods

2.1. Isolation of fungal isolates

Aspergillus versicolor was utilized for the biosynthesis of nanoparticles as it exhibited a great potency to biosynthesize both investigated nanoparticles among the 10 tested fungal isolates. *A. versicolor* was isolated as an endophyte from sand lily (*Pancratium maritimum* L.) leaves [29], as previously described by Kumar et al. [30], while aflatoxigenic *A. flavus* was isolated from peanut (*Arachis hypogaea* L.) seeds according to earlier report [31].

2.2. Molecular identification of isolated fungi

Czapek Dox broth medium was used to culture the pure fungal isolates for 5 d at 28°C. Total DNA was extracted from each isolate using a specific kit "Norgen Plant/Fungi DNA Isolation Kit (Sigma, Thorold, Canada)" [32]. To amplify the ITS region of the selected strains, universal primers ITS-1 (5′-TCC GTA GGT GAA CCT GCG G-3′) and ITS-4 (5′-TCC TCC GCT TAT TGA TAT GC-3′) were employed, as previously described by Mohamed et al. [33]. PCR amplification was performed following the same protocol as earlier described by Hassan et al. [32].

2.3. Preparation of mycelial-free culture filtrate

The fungal biomass was cultivated aerobically in PD broth and incubated for 5 d at 28°C in an orbital shaker with constant shaking at 150 rpm/min. Subsequently, the fungal biomass obtained was then filtered by using a Whatman no. 1 filter paper, and the resultant biomass was washed numerous times with double distilled water. Then, 10 g of fungal mycelia were soaked into 200 mL sterile double distilled water in a 500 mL Erlenmeyer flask and was further incubated at 28°C for 48 h with gentle shaking at 120 rpm. The filtrate was then used for nanoparticle synthesis.

2.4. Mycosynthesis of silver and gold nanoparticles

Stock solutions of both silver nitrate and gold chloride (hydrogen tetrachloroaurate (III) hydrate ($HAuCl_4{\cdot}3H_2O$) were prepared in deionized water, and the solutions were then individually added to the mycelial-free filtrate, resulting in a final concentration of 1 mM. The flask was then kept in dark condition at 28°C for 72 h. Gold chloride solution and fungal filtrate served as negative controls. The resulted nanoparticles were collected by centrifugation and freeze-dried by lyophilization, and a certain weight was disseminated by using ultra-sonication in sterile double distilled water for use as stock solutions.

2.5. Characterization of AuNPs and AgNPs

2.5.1. UV–visible (UV–vis) spectroscopy

The formation of AgNPs and AuNPs was determined by visual observation of color change that indicates the reduction reaction, and AgNPs and AuNPs were established by UV–vis spectroscopy (Jasco V-530) for the occurrence of distinguishable surface plasmon resonance bands of AgNPs and AuNPs.

2.5.2. Transmission electron microscopy (TEM)

The morphology of newly synthesized AgNPs and AuNPs were analyzed by a transmission electron microscope (JEOL/JEM-2100, HRTEM, Tokyo, Japan). The examined TEM specimen was concocted by drop-casting and dissemination of AgNPs and AuNPs on copper grids, and the samples were then dried at ambient temperature.

2.5.3. Fourier transform infrared spectroscopy (FTIR)

FTIR (6100, Perkin-Elmer, Germany) was utilized to investigate the functional groups on the surface of AgNPs and AuNPs at 4 cm^{-1} resolution and 400–4000 cm^{-1} wavelength range.

2.5.4. X-ray diffraction (XRD) analysis

The freeze-dried powders were subjected for XRD analysis for the presence of elemental AgNPs and AuNPs, and the experiments were performed on a X-ray diffractometer (Panalytical X'PERT PRO) with Cu kα- radiation (λkα = 1. 1.540562 Å) run at 30 mA and 40 kV and scanning diffraction style in the 2∅ of 5-90° range.

2.6. Impact of AgNPs and AuNPs and their mixture on the growth and aflatoxin B_1 accumulation of aflatoxigenic A. flavus strain

Dilutions of the stock solutions of AgNPs and AuNPs were prepared using sterilized deionized H_2O to attain the desired concentrations (10000, 5000, 3000, 1000, 750, 500, 250, and 125 μg/mL) used for antimycotic and antiaflatoxigenic investigation. The dry weight of the fungal biomass in each NPs treatment was then recorded and compared with the control. All experiments were repeated three times [27]. Aflatoxin B_1 was purified and detected using the thin-layer chromatographic (TLC) technique [34,35].

2.6.1. Determination of AFB_1 by high performance liquid chromatography (HPLC)

The concentration of AFB1 was determined by HPLC [36].

2.7. Radical scavenging activity by 1,1-diphenyl-2-picryl-hydrazyl (DPPH) assay

The antioxidant properties of AgNPs and AuNPs were measured as scavenging activity or as a hydrogen donating form based on the procedure reported by Brand-Williams et al. [37] and Adebayo et al. [38] with minor modifications (Fig. S1).

2.8. Data analysis

Statistical analysis was performed using SPSS (version 16), and the differences were analyzed by one-way ANOVA. The values were expressed as mean ± SE, and the significance level was considered as 0.05.

3. Results

3.1. Fungal isolates and phylogenetic analysis

According to the phenotypic and phylogenetic characteristics, *A. versicolor* was identified as an endophyte from the leaves of *Pancratium maritimum*, while *A. flavus* was identified as an isolate from the seeds of *Arachis hypogaea*. Both the isolates were identified by performing ITS region sequencing, and the sequences obtained for the ITS regions were further subjected to a BLAST search at the NCBI database. The two isolates were identified as *Aspergillus versicolor* TU-63 (GenBank accession no. OL411612) and *A. flavus* TU-61(GenBank accession no. OL411610) (Fig. 1).

Nucleotide comparisons of the ITS regions among the *Aspergillus* and other similar strains revealed that the *A. versicolor* TU-63 strain exhibited 100% and 98% similarity with the strains *A. versicolor* MK722085 and *A. versicolor* MT609910 from the GenBank, respectively. On the other hand, 99 and 98% identity was observed between *Aspergillus flavus* TU-61 and *A. flavus* MZ052072 and *A. flavus* MZ018647, respectively. *Aspergillus flavus* TU-61 also showed approximately 97% and 96% similarity with *A. flavus* MW193211 and *A. flavus* MW193310, respectively.

3.2. Characterization of mycosynthesized AuNPs and AgNPs

The bioreduction of $AgNO_3$ was noticed by visual examination of the culture filtrate after 2 d of incubation with a color change to deep brown, while the color change in the solution containing gold chloride and mycelia filtrate to purple indicated biogenesis of AuNPs (Fig. 2A).

UV–Vis wave analysis of AgNPs over the range of 200–600 nm revealed that the surface plasmon resonance band originated at 432 nm. Absorption measurements over the range of 300–700 nm for AuNPs produced a peak at 536 nm, coinciding to the plasmon absorbance of AuNPs (Fig. 2B).

The size and morphology examined by TEM showed that the formed AgNPs were monodispersed with a relatively regular spherical structures and an average particle size of 5–37 nm. TEM analysis of the biosynthesized AuNPs revealed that they were polydispersive showing spherical and hexagonal structures with a particle size range of 37–62 nm (Fig. 2C).

The crystalline quality of AgNPs was determined by the XRD analysis that exposed the typical face-centered cubic (fcc) structure of the metal silver. The XRD spectra revealed four major Bragg diffraction peaks at 2θ values of 38.121°, 44.308°, 64.458°, and

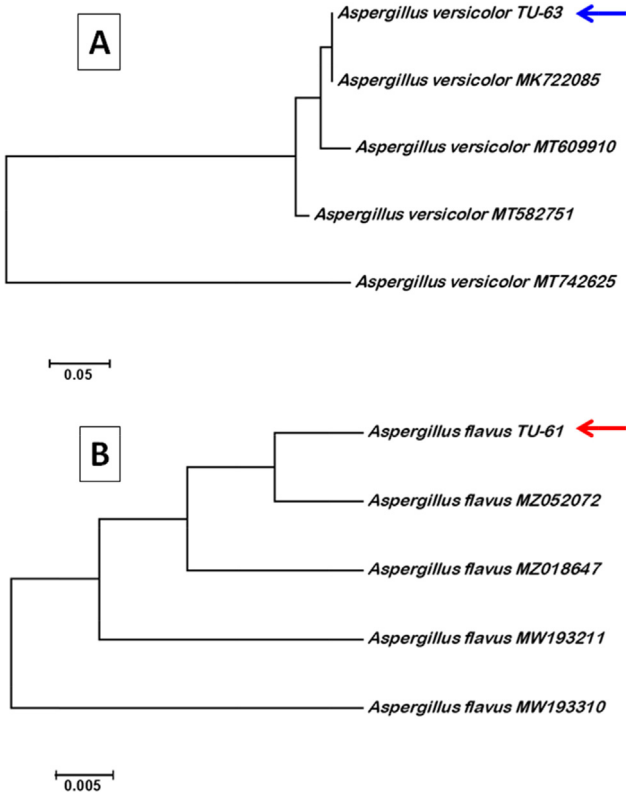

Fig. 1. Neighbor-joining phylogenetic tree of the ITS sequences of the isolated fungal strains with the sequences of closely related strains: (A) the phylogenetic tree of *A. versicolor* and (B) the phylogenetic tree of *A. flavus*.

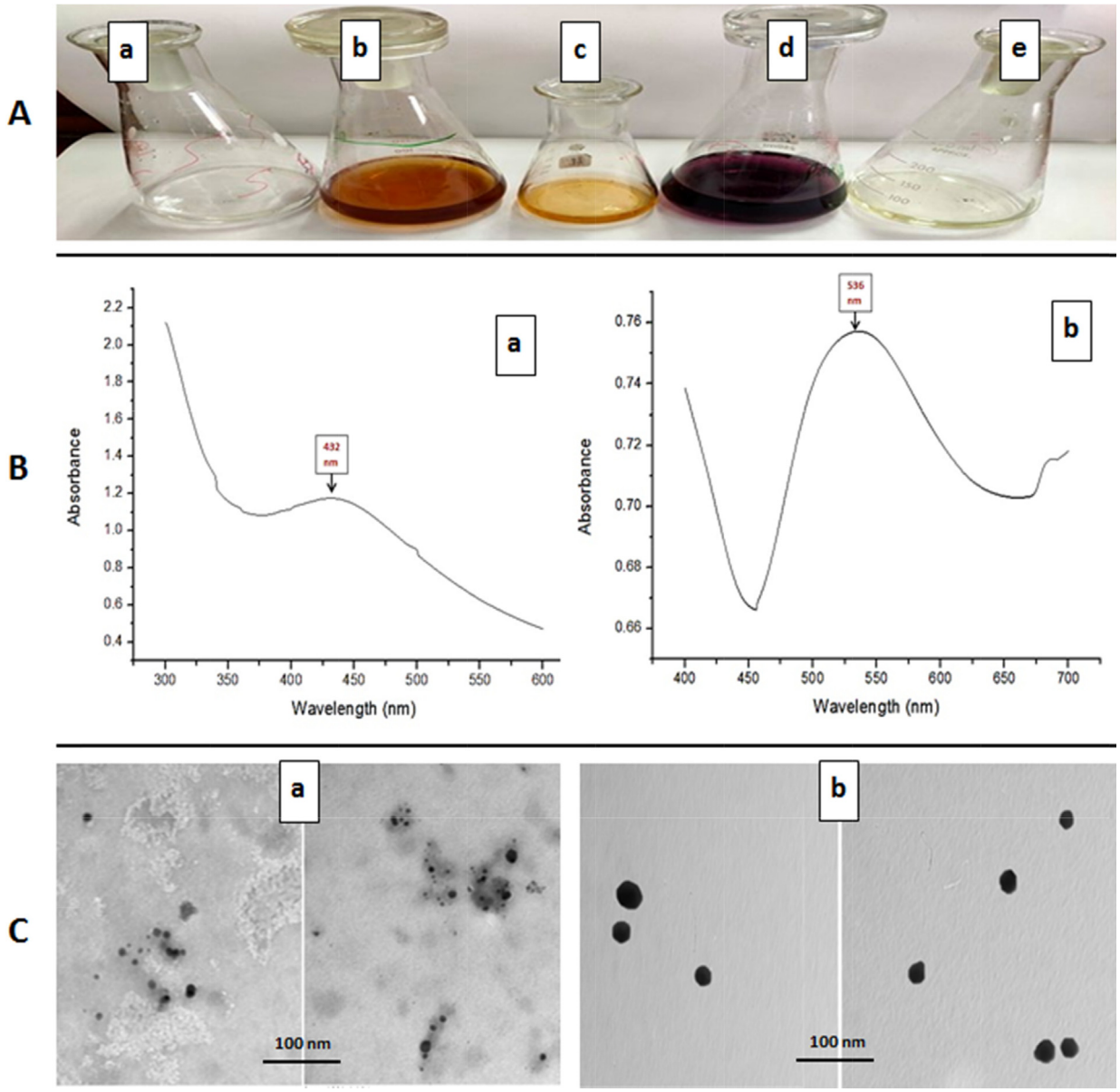

Fig. 2. (A) Color change of mycosynthesized AgNPs and AuNPs (a) silver nitrate, (b) AgNPs, (c) *A. versicolor* mycelial filtrate, (d) AuNPs, and (e) gold chloride; (B) UV–Vis absorption spectrum of biosynthesized (a) AgNPs and (b) AuNPs; (C) TEM images of (a) AgNPs and (b) AuNPs.

77.415° that matched to the (111), (200), (220), and (311) planes of fcc Ag, respectively. The diffraction peaks were harmonious with the (JCPDS card No. 04–0783) standard database files, which confirm that the mycosynthesized AgNPs had a crystalline nature (Fig. 3A). XRD analysis of AuNPs exhibited Bragg diffraction peaks and planes of fcc as for AgNPs by employing (space group Fm3 m, JCPDS File NO. 89–3697) standard database files (Fig. 3B).

The FTIR spectrum of AgNPs showed a number of different bands including strong bands that appeared in the spectrum such as the band centered at 2965.86 and 2903.53 cm^{-1} for aliphatic C—H stretching and the strong band at 1547.36 cm^{-1} for carbonyl group C=O stretching. The band centered at 1292.03 is attributed for the C—O stretching group, while the strong band centered at 1053.73 is attributed to the S=O stretching functional group in the sample (Fig. 4A).

The FTIR spectrum of AuNPs showed a number of different bands including strong bands that appeared in the spectrum such as the band centered at 2972.08 and 2900.92 cm^{-1} for aliphatic C—H stretching. The strong band centered at 1053.73 was attributed to the S=O stretching functional group in the sample. A small peak was observed at 3658.98 cm^{-1}, which could be because of the presence of a —O—H hydroxyl group. The band centered at 1596.09 cm^{-1} was attributed to carbonyl group C=O stretching (Fig. 4B). These bands indicated that those functional groups were able to bind ions of the silver and gold metals and can biosynthesize and capping AgNPs and AuNPs to block clustering and settle the medium.

3.3. Impacts of AgNPs and AuNPs and Ag-AuNPs treatment on the growth of Aspergillus flavus and its capability to produce aflatoxin B_1

The impacts of AgNPs, AuNPs, and their mixture to inhibit the outgrowth and aflatoxins B_1 biosynthesis by *A. flavus* were observed (Table 1 and Fig. S1-S20). The present study revealed that the impacts of AgNPs, AuNPs, and their mixture in inhibiting the growth and aflatoxin B_1 production capability of *A. flavus*. The growth inhibition was determined by dry weight, where it ranged between 0–1.55 g at 10000–125 μg/mL AgNPs, 0–1.42 g at 10000–

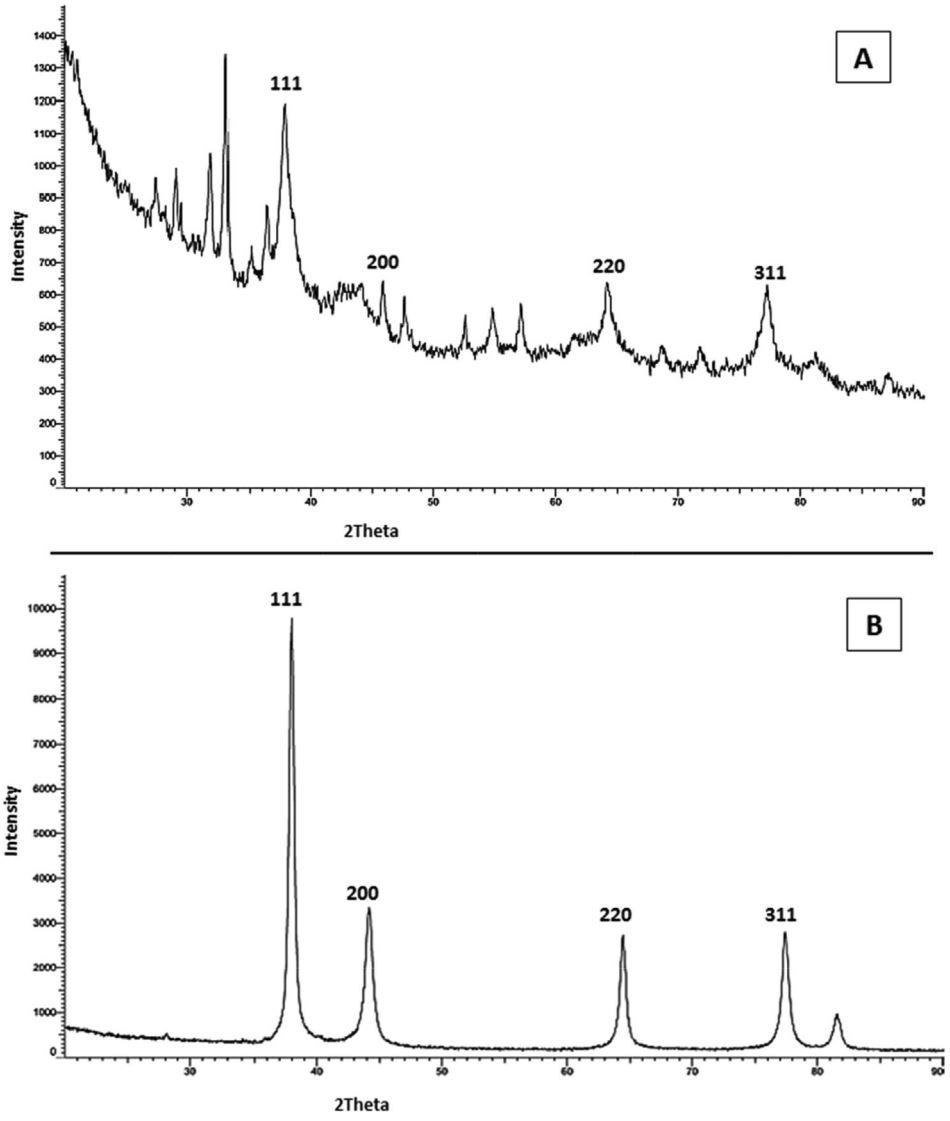

Fig. 3. XRD micrograph of mycosynthesized (A) AgNPs and (B) AuNPs.

125 μg/mL AuNPs, and 0–1.62 g at 10000–125 μg/mL Ag-AuNPs in comparison to the control (1.73 g). Our study also revealed that the inhibition of growth and aflatoxin B_1 production capability of *A. flavus* was directly linked to the concentrations of the nanoparticles tested. The quantities of accumulated aflatoxin B_1 decreased when the used nanoparticles concentration increased. The growth of *A. flavus* was completely inhibited at 10000 μg/mL concentration, while no aflatoxin B_1 production occurred at 10,000 and 5000 μg/mL of AgNPs, AuNPs, and their mixture, respectively. The concentration that showed no aflatoxin B1 production was less than those for the reduction of fungal growth. The highest concentration for the inhibition of aflatoxin B_1 production (99.55, 99.999, and 99.59%) for AgNPs, AuNPs, and Ag-AuNPs, respectively, was 3000 μg/ml, whereas fungal growth was decreased significantly at these concentrations. The lowest concentration for the inhibition of aflatoxin B_1 formation (60.50, 67.33, and 23.24%) for AgNPs, AuNPs, and Ag-AuNPs, respectively, was 125 μg/mL, whereas fungal growth was reduced significantly at these concentrations (Fig. 5A, B).

3.4. Antioxidant activity of AgNPs, AuNPs, and Ag-AuNPs

The mycosynthesized AgNPs exhibited satisfactory antiradical activities as compared to BHT with inhibitions of 27.02–79.58%, AuNPs displayed inhibitions of 40.19–80.22%, while Ag-AuNPs displayed inhibitions of 33.59–76.85% at the tested concentrations (12.5–100 μg/mL) (Table 2).

4. Discussion

In this study, we attempted to synthesize AuNPs and AgNPs by *Aspergillus versicolor* isolated as an endophyte from the leaves of *Pancratium maritimum*, while aflatoxigenic *A. flavus* was isolated from the seeds of *Arachis hypogaea*. Both fungi were identified on the basis of the phenotypic and phylogenetic characteristics. The ITS loci are the most credible regions for identifying strains at the species level. Not surprisingly, ITS region sequencing is reported as a powerful alternative method for accurate molecular identification of *Aspergillus* strains to the species level [32].

AgNPs biosynthesis was indicated by the change in color of the culture filtrate from faint xanthous to deep brown color, while pur-

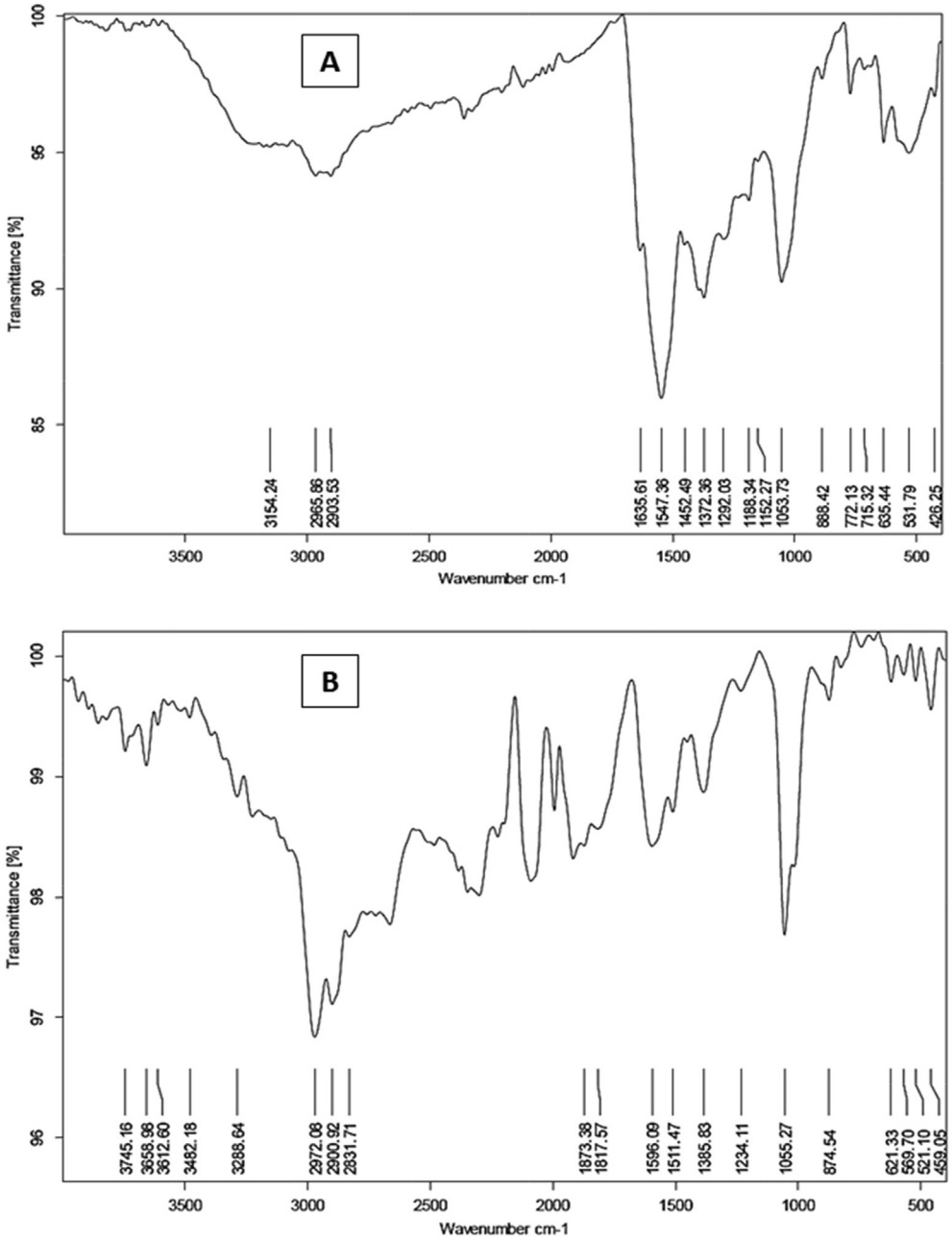

Fig. 4. FTIR analysis of biosynthesized (A) AgNPs and (B) AuNPs.

Table 1
Effects of different concentrations of biosynthesized AgNPs, AuNPs, and their mixture on the growth of *A. flavus* and accumulation of AFB_1.

NPs conc. (μg/mL)	AgNPs			AuNPs			Ag-AuNPs		
	Growth	AFB_1		Growth	AFB1		Growth	AFB_1	
	Dry weight (g)	Quantity (ng/100 ml)	Reduction (%)	Dry weight (g)	Quantity (ng/100 ml)	Reduction (%)	Dry weight (g)	Quantity (ng/100 ml)	Reduction (%)
Control	1.73 ± 0.02[a]	8787	0	1.73 ± 0.02[a]	8787	0	1.73 ± 0.02[a]	8787	0
10,000	0.00 ± 0.00[p]	0	100	0.00 ± 0.00[p]	0	100	0.00 ± 0.00[p]	0	100
5000	0.49 ± 0.01[n]	0	100	0.38 ± 0.01[o]	0	100	0.49 ± 0.01[n]	0	100
3000	0.67 ± 0.02 [k]	39.6	99.55	0.62 ± 0.01 [l]	0.11	99.999	0.57 ± 0.01 [m]	36	99.59
1000	0.85 ± 0.01[j]	91.5	98.96	0.82 ± 0.01[j]	42.3	99.52	0.67 ± 0.01 [k]	247	97.19
750	0.97 ± 0.01 [h]	274	96.88	0.92 ± 0.01[i]	230	97.38	0.83 ± 0.02[j]	797	90.93
500	1.09 ± 0.01[f]	308	96.49	1.08 ± 0.01[f]	271	96.92	1.02 ± 0.01 [g]	1280	85.43
250	1.45 ± 0.01[d]	1414	83.91	1.20 ± 0.01[e]	859	90.22	1.19 ± 0.03[e]	6138	30.15
125	1.55 ± 0.03[c]	3471	60.50	1.42 ± 0.01[d]	2871	67.33	1.62 ± 0.02[b]	6745	23.24

The data are expressed as mean value of three replicates ± SE. Values followed by different letters are significantly different at $p < 0.05$.

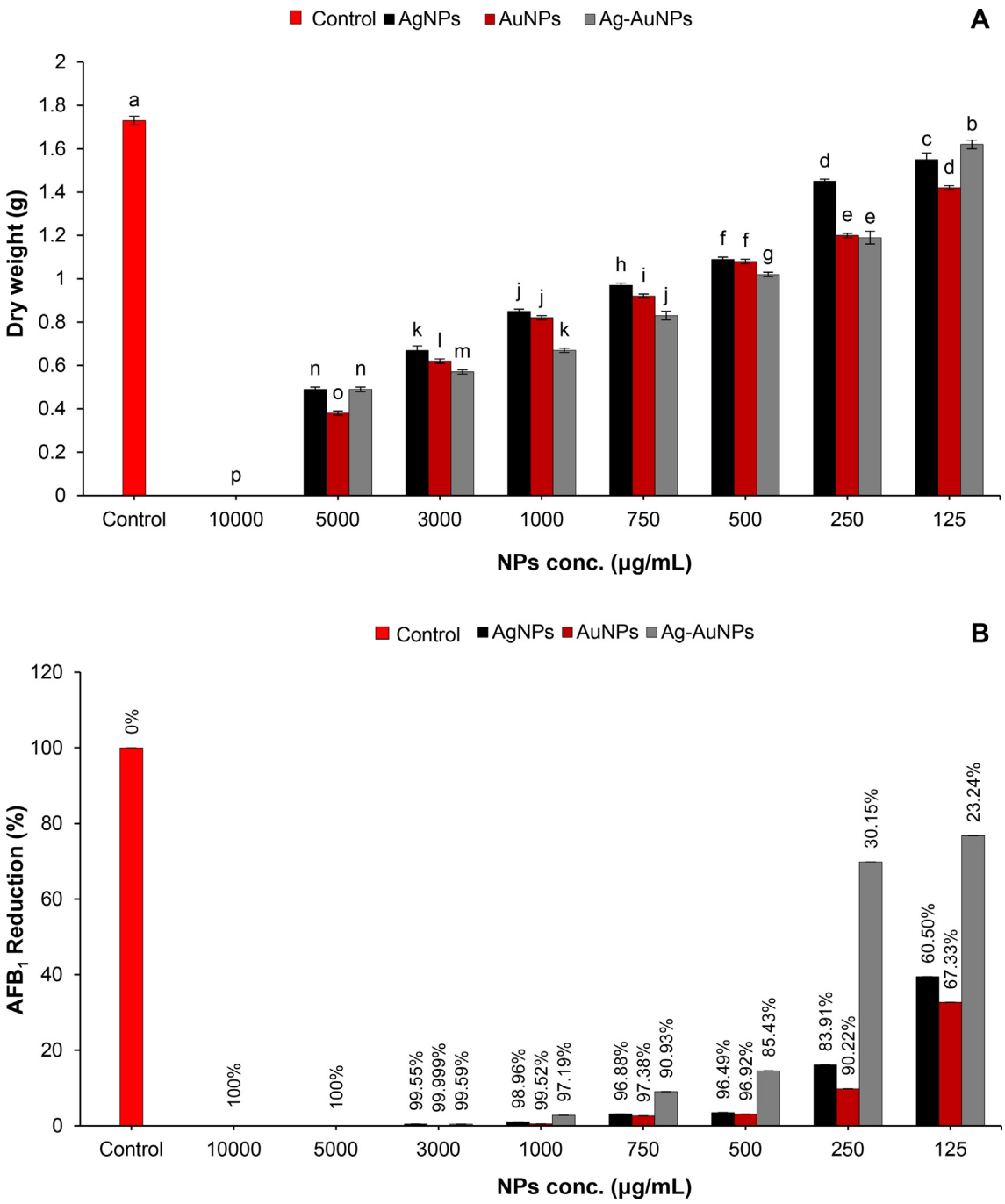

Fig. 5. Effects of different concentrations of biosynthesized AgNPs, AuNPs, and their mixture on (A) the outgrowth of *A. flavus* and (B) AFB_1 production.

Table 2
DPPH radical scavenging activities (%) of mycosynthesized AgNPs, AuNPs, and Ag-AuNPs.

Test NPs	Concentration (µg/mL)							
	1000	500	300	100	75	50	25	12.5
AgNPs	79.58 ± 0.36^{b}	76.18 ± 0.30^{c}	65.87 ± 0.17^{c}	60.14 ± 0.18^{c}	56.98 ± 0.29^{c}	48.08 ± 0.26^{c}	41.68 ± 0.60c	27.02 ± 0.64^{c}
AuNPs	80.22 ± 0.22^{b}	76.82 ± 0.08^{b}	69.64 ± 0.18^{b}	67.22 ± 0.21^{b}	64.05 ± 0.17^{b}	60.82 ± 0.01^{b}	56.28 ± 0.24b	40.19 ± 1.13^{b}
Ag-AuNPs	76.85 ± 0.97^{c}	69.17 ± 0.07^{d}	65.13 ± 0.52^{c}	58.49 ± 0.16^{d}	55.59 ± 0.50^{d}	44.68 ± 0.19^{d}	32.58 ± 0.53d	33.59 ± 0.33^{d}
BHT	94.17 ± 0.23^{a}	90.57 ± 0.17^{a}	83.96 ± 0.54^{a}	78.87 ± 0.37^{a}	73.21 ± 0.51^{a}	69.17 ± 0.07^{a}	65.13 ± 0.52^{a}	60.14 ± 0.18^{a}

The data are expressed as mean values of three replicates ± SE. Values followed by different letters are significantly different at $p < 0.05$.

ple color mycelial filtrate was indicative of AuNPs biosynthesis; these observations are in line with those reported by earlier studies [39,40]. The bioreduction of silver ions into silver-NPs is monitored by extracellular enzymes secreted by fungi [41] and in the case of bioreduction of gold ions [42].

UV–Vis spectroscopic analyses of AgNPs revealed the surface plasmon resonance band at 432 nm, while for AuNPs, surface plasmon absorbance peak was observed at 536 nm. These observations are in accordance with previous studies, where UV–visible absorbance peak at 420 nm was observed for the fungal filtrate containing AuNPs [43,44], which reported that mycosynthesized gold nanoparticles exhibited a peak corresponding to 550 nm in the absorption spectrum. The size and morphology analysis of AgNPs and AuNPs by TEM showed that AgNPs formed were monodispersed, showing relatively stable spherical structures with an average size of 5–37 nm, while AuNPs were polydispersive, showing spherical and hexagonal structures with a particle size range of 37–62 nm. These observations concur with Elgorban et al. [45] who synthesized AgNPs by using a soil isolate of *Aspergillus versicolor*, which were characterized as spherical shape nanoparticles with the size ranging from 5 to 30 nm, and with Abd El-Kareem and Zohri [40] who analyzed TEM images of mycosynthesized AuNPs and showed that they were well dispersed with spherical, pentagonal, and hexagonal shapes covering a size range of 5–30 nm.

Next, XRD analyses of the newly formed AgNPs and AuNPs were conducted. The crystalline quality of AgNPs was confirmed by XRD analyses, which revealed the typical fcc structure of the metal silver, while AuNPs exhibited Bragg diffraction peaks and planes of fcc in XRD analyses.

We also performed FTIR analyses of AgNPs and AuNPs to ascertain the major functional groups bound to the AgNPs and AuNPs. Several different bands were observed for both AgNPs and AuNPs at different wavelengths. For AgNPs, the band centered at 2965.86 and 2903.53 cm^{-1} indicated aliphatic C—H stretching; a strong band at 1547.36 cm^{-1} represented carbonyl group C═O stretching, while bands centered at 1292.03 and 1053.73 cm^{-1} were attributed to the C—O stretching and S═O stretching functional groups in the sample. Similarly, for AuNPs, the band centered at 2972.08 and 2900.92 cm^{-1} showed aliphatic C—H stretching, while the band at 1053.73 cm^{-1} is linked to a S═O stretching. The other functional groups identified in the sample were —O—H hydroxyl group and carbonyl group C═O based on the presence of a weak band centered at 3658.98 cm-^{1} (for hydroxyl group) and a band centered at 1596.09 cm^{-1} (for carbonyl group). These bands indicated that these functional groups are better able to bind ions of the silver and gold metals and can biosynthesize and cap AgNPs and AuNPs to block clustering and settle the medium. According to an earlier report [46], AgNPs are bound to proteins through free carboxylic or amine groups, whilst the incidence of a peak at C═O stretching confirms the existence of carboxylic groups in the substances that are attached to AuNPs. The role of extracellular proteins in the biosynthesis of AuNPs is supported by the presence of standard FTIR spectra of proteins and peptides [47].

The effectiveness of the AgNPs, AuNPs, and their mixture to inhibit the growth and aflatoxin B_1 synthesis ability of *A. flavus* was analyzed next. Our data clearly show that the nanoparticles inhibited the growth of *A. flavus* and aflatoxin B_1 in a concentration-dependent manner. These results were expected because when AgNPs come in contact with the fungal plasma membrane, they perforate the membrane, resulting in the seepage of ions and low molecular weight compounds. Subsequently, the silver-NPs then disrupt the respiratory chain, which is then followed by halting of cell division, ultimately resulting in cell death [48]. After AgNPs treatment, the fungal genome loses its capacity to replicate, and transcription and adenine triphosphate synthesis could be promoted [49]. When *A. flavus* is treated with AgNPs, the expression levels of *omt-A* gene, which encodes enzymes encompassed in the aflatoxins biosynthesis pathway, are reduced [50]. The antimicrobial specificity of the nanoparticles is also correlated to their total surface area; thus, the smaller the particles in size, the quicker will be their penetration in microbial cells [51].

Antioxidants are vital in decreasing the intracellular levels of reactive oxygen species, which lowers the intracellular oxidative level that in turn affects the signaling of the aflatoxin biosynthesis pathway, followed by significant suppression of aflatoxins production by *A. flavus*. In our study, at the concentrations between 12.5–100 μg/mL, AgNPs showed antiradical activity of 27.02–79.58%, while AuNPs and Ag-AuNPs showed antiradical activity of 40.19–80.22% and 33.59–76.85%, respectively. The functional groups of the biomolecules attached to the particle's surface could be accountable for the antioxidant potency of the biofabricated AgNPs through their bioreductant capacity [52]. Antioxidants exerted a significant influence on AFB_1 accumulation by *A. flavus* [53]. Phytosynthesized silver, gold, and silver-gold nanoparticles displayed satisfactory DPPH-scavenging activities that were dose-dependent at the tested concentrations [38].

5. Conclusions

In the present study, *Aspergillus versicolor* was used to biosynthesize AgNPs and AuNPs. Mycosynthesized NPs were characterized by UV–vis spectroscopy, XRD, TEM, and FTIR. Data obtained from the present investigation suggest that mycosynthesized AgNPs, AuNPs, and Ag-AuNPs exerted antifungal and antiaflatoxigenic ability against *A. flavus* and antioxidant activity using DPPH assay. More studies are required to estimate the influence and application of mycosynthesized metallic nanoparticles against different mycotoxigenic fungi, particularly for food products.

Author Contributions

- Study conception and design: H Sheikh; MF Awad
- Data collection: H Sheikh; MF Awad
- Analysis and interpretation of results: H Sheikh; MF Awad
- Draft manuscript preparation: H Sheikh; MF Awad
- Revision of the results and approved the final version of the manuscript: H Sheikh; MF Awad

Financial support

This work was supported by the Deanship of Scientific Research (DSR), King Abdulaziz University, Jeddah [Grant No 725-665-1441].

Conflict of interest

The authors declare no conflict of interest.

Supplementary material

https://doi.org/10.1016/j.ejbt.2022.09.003.

References

[1] Magdi HM, Mourad MHE, Abd El-Aziz MM. Biosynthesis of silver nanoparticles using fungi and biological evaluation of mycosynthesized silver nanoparticles. [cited November 03, 2020]. Egypt J Exp Biol (Bot) 2014;10(1):1–12. , http://www.egyseb.net//?mno=186586.

[2] Endre G, Hegedüs Z, Turbat A, et al. Separation and purification of aflatoxins by centrifugal partition chromatography. Toxins 2019;11(6):309. https://doi.org/10.3390/toxins11060309. PMid: 31151208.

[3] Zein R, Sharrouf W, Selting K. Physical properties of nanoparticles that result in improved cancer targeting. J Oncol 2020;2020:5194780. https://doi.org/10.1155/2020/5194780. PMid: 32765604.
[4] Narayanan KB, Sakthivel N. Biological synthesis of metal nanoparticles by microbes. Adv Colloid Interface Sci 2010;156(1–2):1–13. https://doi.org/10.1016/j.cis.2010.02.001. PMid: 20181326.
[5] Adelere IA, Lateef A. A novel approach to the green synthesis of metallic nanoparticles: the use of agro-wastes, enzymes and pigments. Nanotechnol Rev 2016;5(6):567–87. https://doi.org/10.1515/ntrev-2016-0024.
[6] Lateef A, Ojo SA, Elegbede JA. The emerging roles of arthropods and their metabolites in the green synthesis of metallic nanoparticles. Nanotechnol Rev 2016;5(6):601–22. https://doi.org/10.1515/ntrev-2016-0049.
[7] Akintayo GO, Lateef A, Azeez MA, et al. Synthesis, bioactivities and cytogenotoxicity of animal fur-mediated silver nanoparticles. IOP Conf Ser Mater Sci Eng 2020;805:012041. https://doi.org/10.1088/1757-899X/805/1/012041.
[8] Adelere IA, Lateef A. Microalgal nanobiotechnology and its applications—a brief overview. In: Lateef A, Gueguim-Kana EB, Dasgupta N, editors. Microbial Nanobiotechnology. Materials Horizons: From Nature to Nanomaterials. Singapore: Springer; 2021. p. 233–55. https://doi.org/10.1007/978-981-33-4777-9_8.
[9] Elegbede JA, Lateef A. Microbial Enzymes in Nanotechnology and Fabrication of Nanozymes: A Perspective. In: Lateef A, Gueguim-Kana EB, Dasgupta N, editors. Microbial Nanobiotechnology. Materials Horizons: From Nature to Nanomaterials. Singapore: Springer; 2021. p. 185–232. https://doi.org/10.1007/978-981-33-4777-9_7.
[10] Elegbede JA, Lateef A, Azeez MA, et al. Fungal xylanases-mediated synthesis of silver nanoparticles for catalytic and biomedical applications. IET Nanobiotechnol 2018;12(6):857–63. https://doi.org/10.1049/iet-nbt.2017.0299. PMid: 30104463.
[11] Elegbede JA, Lateef A, Azeez MA, et al. Silver-gold alloy nanoparticles biofabricated by fungal xylanases exhibited potent biomedical and catalytic activities. Biotechnol Prog 2019;35(5):e2829. https://doi.org/10.1002/btpr.2829. PMid: 31050163.
[12] Elegbede JA, Lateef A, Azeez MA, et al. Biofabrication of gold nanoparticles using xylanases through valorization of corncob by *Aspergillus niger* and *Trichoderma longibrachiatum*: antimicrobial, antioxidant, anticoagulant and thrombolytic activities. Waste Biomass Valori 2020;11(3):781–91. https://doi.org/10.1007/s12649-018-0540-2.
[13] Mathiesen JK, Cooper SR, Anker AS, et al. Simple setup miniaturization with multiple benefits for green chemistry in nanoparticle synthesis. Am Chem Soc 2022;7(5):4714–21. https://doi.org/10.1021/acsomega.2c00030. PMid: 35155963.
[14] Balter S. Foodborne Pathogens: Microbiology and Molecular Biology. Emerg Infect Dis 2006;12(12):2003. https://doi.org/10.3201/eid1212.061077.
[15] Jalili M. A review on aflatoxins reduction in food. [cited June 09, 2021]. Iranian J Health Saf Environ 2015;3(1):445–59. , http://www.ijhse.ir/index.php/IJHSE/article/view/136.
[16] Dors GC, Caldas SS, Feddern V, et al. Aflatoxins: Contamination, analysis and control. In: Guevara-González RG, editor. Aflatoxins: Biochemistry and Molecular Biology, vol. 20. London: IntechOpen; 2011. p. 415–38. https://doi.org/10.5772/24902.
[17] Santini A, Raiola A, Meca G, et al. Aflatoxins, ochratoxins, trichothecenes, patulin, fumonisins and beauvericin in finished products for human consumption. J Clin Toxicol 2015;5(4):265. https://doi.org/10.4172/2161-0495.1000265.
[18] Varga J, Frisvad JC, Samson RA. Two new aflatoxin producing species, and an overview of *Aspergillus* section *Flavi*. Stud Mycol 2011;69(1):57–80. https://doi.org/10.3114/sim.2011.69.05. PMid: 21892243.
[19] Lateef A, Gueguim-Kana EB. Quality assessment and hazard analysis in the small-scale production of poultry feeds in Ogbomoso, Southwest. Nigeria Qual Assur Saf Crops Foods 2014;6(1):105–13. https://doi.org/10.3920/QAS2012.0209.
[20] Ceniti C, Costanzo N, Spina AA, et al. Fungal contamination and aflatoxin B1 detected in hay for dairy cows in South Italy. Front Nutr 2021;8:704976. https://doi.org/10.3389/fnut.2021.704976. PMid: 34621772.
[21] Chawanthayatham S, Valentine CC, Fedeles BI, et al. Mutational spectra of aflatoxin B1 *in vivo* establish biomarkers of exposure for human hepatocellular carcinoma. Proc Natl Acad Sci USA 2015;114(15):3101–9. https://doi.org/10.1073/pnas.1700759114. PMid: 28351974.
[22] International Agency for Research on Cancer (IARC). Personal habits and indoor combustions. [cited June 09, 2021]. Volume 100 E.A review of human carcinogens: IARC Monogr. Eval. Carcinog. Risks Hum 2012; 100(Pt E), 1-538. https://pubmed.ncbi.nlm.nih.gov/23193840/PMid:23193840.
[23] European Commission (EC). Commission Regulation No 401/2006 of 23 February 2006 laying down the methods of sampling and analysis for the control of the levels of mycotoxins in foodstuffs. Official J Eur Union 2006;70:12–34.
[24] Adeyeye SAO. Aflatoxigenic fungi and mycotoxins in food: a review. Crit Rev Food Sci Nutrit 2019;60(5):709–21. https://doi.org/10.1080/10408398.2018.1548429. PMid: 30689400.
[25] Peles F, Sipos P, Kovács S, et al. Biological control and mitigation of aflatoxin contamination in commodities. Toxins 2021;13(2):104. https://doi.org/10.3390/toxins13020104. PMid: 33535580.
[26] Rai M, Yadav A, Gade A. Silver nanoparticles as a new generation of antimicrobials. Biotechnol Adv 2009;27(1):76–83. https://doi.org/10.1016/j.biotechadv.2008.09.002. PMid: 18854209.
[27] AbdEl-Kareem MM, Zohri AA. Inhibition of three toxigenic fungal strains and their toxins production using selenium nanoparticles. Czech Mycol 2017;69(2):193–204. https://doi.org/10.33585/cmy.69206.
[28] Mousavi SAA, Pourtalebi S. Inhibitory effects of silver nanoparticles on growth and aflatoxin B1 production by *Aspergillus parasiticus*. [cited July 02, 2021]. Iran J Med Sci 2015;40(6):501–6. PMID: 26538778 https://www.ncbi.nlm.nih.gov/pmc/articles/PMC4628140/.
[29] Mohamed E, Kasem AMM, Farghali KA. Seed germination of Egyptian *Pancratium maritimum* under salinity with regard to cytology, antioxidant and reserve mobilization enzymes, and seed anatomy. Flora 2018;242:120–7. https://doi.org/10.1016/j.flora.2018.03.011.
[30] Kumar S, Kaushik N, Edraba-Ebel R, et al. Isolation, characterization, and bioactivities of endophytic fungi of *Tylophora indica*. World J Microbiol Biotechnol 2011;27(3):571–7. https://doi.org/10.1007/s11274-010-0492-6.
[31] El-Maghraby OMO, El-Maraghy SSM. Mycoflora and mycotoxins of peanut (*Arachis hypogaea* L.) seeds in Egypt. I- Sugar fungi and natural occurrence of mycotoxins. Mycopathologia 1987;98(3):165–70. https://doi.org/10.1007/BF00437651. PMid: 3587340.
[32] Hassan MM, Farid MA, Gaber A. Rapid identification of *Trichoderma koningiopsis* and *Trichoderma longibrachiatum* using sequence characterized amplified region markers. Egypt J Biol Pest Control 2019;29(1):13. https://doi.org/10.1186/s41938-019-0113-0.
[33] Mohamed H, El-Shanawany AR, Shah AM, et al. Comparative analysis of different isolated oleaginous Mucoromycota fungi for their γ-linolenic acid and carotenoid production. Biomed Res Int 2020;2020:3621543. https://doi.org/10.1155/2020/3621543. PMid: 33204691.
[34] El-Gohary AH. Study on aflatoxins in some foodftuffs with special reference to public health hazard in Egypt. Asian-Australas J Anim Sci 1995;8(6):571–5. https://doi.org/10.5713/ajas.1995.571.
[35] Yazdani D, Zainal AMA, Tan YH, et al. Evaluation of the detection techniques of toxigenic *Aspergillus isolates*. Afric J Biotechnol 2010;9(45):7654–9.
[36] Abdel-Rahman GN, Sultan YY, Salem SH, et al. Identify the natural levels of mycotoxins in Egyptian roasted peanuts and the destructive effect of gamma radiation. J Microbiol Biotechnol Food Sci 2019;8(5):1174–7. https://doi.org/10.15414/jmbfs.2019.8.5.1174-1177.
[37] Brand-Williams W, Cuvelier ME, Berset C. Use of a free radical method to evaluate antioxidant activity. LWT Food Sci Technol 1995;28(1):25–30. https://doi.org/10.1016/S0023-6438(95)80008-5.
[38] Adebayo EA, Ibikunle JB, Oke AM, et al. Antimicrobial and antioxidant activity of silver, gold and silver-gold alloy nanoparticles phytosynthesized using extract of Opuntia ficus-indica. Rev Adv Mater Sci 2019;58(1):313–26. https://doi.org/10.1515/rams-2019-0039.
[39] Sadowski Z, Maliszewska IH, Grochowalska B, et al. Synthesis of silver nanoparticles using microorganisms. Mater Sci Pol 2008;26(2):419–24.
[40] Abdel-Kareem MM, Zohri AA. Extracellular mycosynthesis of gold nanoparticles using *Trichoderma hamatum:* optimization, characterization and antimicrobial activity. Lett Appl Microbiol 2018;67(5):465–75. https://doi.org/10.1111/lam.13055. PMid: 30028030.
[41] Yassin MA, El-Samawaty AMA, Dawoud TM, et al. Characterization and anti-*Aspergillus flavus* impact of nanoparticles synthesized by *Penicillium citrinum*. Saudi J Biol Sci 2017;24(6):1243–8. https://doi.org/10.1016/j.sjbs.2016.10.004. PMid: 28855817.
[42] Dhanasekar NN, Rahul GR, Narayanan KB, et al. Green chemistry approach for the synthesis of gold nanoparticles using the fungus *Alternaria* sp. J Microbiol Biotechnol 2015;25(7):1129–35. https://doi.org/10.4014/jmb.1410.10036. PMid: 25737119.
[43] Abdel-Hadi AM, Awad MF, Abo-Dahab NF, et al. Extracellular synthesis of silver nanoparticles by *Aspergillus terreus*: Biosynthesis, characterization and biological activity. Biosci Biotechnol Res Asia 2014;11(3):1179–86. https://doi.org/10.13005/bbra/1503.
[44] Honary S, Gharaei-Fathabad E, Barabadi H, et al. Fungus-mediated synthesis of gold nanoparticles: A novel biological approach to nanoparticle synthesis. Nanosci Nanotechnol 2013;13(2):1427–30. https://doi.org/10.1166/jnn.2013.5989. PMid: 23646653.
[45] Elgorban AM, Aref SM, Seham SM, et al. Extracellular synthesis of silver nanoparticles using *Aspergillus versicolor* and evaluation of their activity on plant pathogenic fungi. Mycosphere 2016;7(6):844–52. https://doi.org/10.5943/mycosphere/7/6/15.
[46] Philip D. Biosynthesis of Au, Ag and Au–Ag nanoparticles using edible mushroom extract. Spectrochim Acta A: Mol Biomol Spectrosc 2009;73(2):374–81. https://doi.org/10.1016/j.saa.2009.02.037. PMid: 19324587.
[47] Thakker JN, Dalwadi P, Dhandhukia PC. Biosynthesis of gold nanoparticles using *Fusarium oxysporum* f. sp. *cubense* JT1, a plant pathogenic fungus. Int Scholarly Res Notices 2013;2013:515091. https://doi.org/10.5402/2013/515091. PMid: 25969773.
[48] Manjumeena R, Duraibabu D, Sudha J, et al. Biogenic nanosilver incorporated reverse osmosis membrane for antibacterial and antifungal activities against selected pathogenic strains: an enhanced eco-friendly water disinfection approach. J Environ Sci Health A: Tox Hazard Subst Environ Eng 2014;49(10):1125–33. https://doi.org/10.1080/10934529.2014.897149. PMid: 24844893.

[49] Kim SW, Jung HJ, Lamsal K, et al. Antifungal effects of silver nanoparticles (AgNPs) against various plant pathogenic fungi. Mycobiology 2012;40 (1):415–27. https://doi.org/10.5941/MYCO.2012.40.1.053. PMid: 22783135.
[50] Deabes MM, Khalil WKB, Attallah AG, et al. Impact of silver nanoparticles on gene expression in *Aspergillus flavus* producer aflatoxin B1. Open Access Maced J Med Sci 2018;6(4):600–5. https://doi.org/10.3889/oamjms.2018.117. PMid: 29731923.
[51] Martinez-Gutierrez F, Olive PL, Banuelos A, et al. Synthesis, characterization, and evaluation of antimicrobial and cytotoxic effect of silver and titanium nanoparticles. Nanomedicine 2010;6(5):681–8. https://doi.org/10.1016/j.nano.2010.02.001. PMid: 20215045.
[52] Bhakya S, Muthukrishnan S, Sukumaran M, et al. Biogenic synthesis of silver nanoparticles and their antioxidant and antibacterial activity. Appl Nanosci 2015;6(5):755–66. https://doi.org/10.1007/s13204-015-0473-z.
[53] Hassane AMA, Abo-Dahab NF, El-Shanawany AA, et al. *In vitro* and *in situ* impact of safe synthetic and natural antioxidants on populations and aflatoxin B1 accumulation by A*spergillus flavus*. Biotechnol Sci Res 2018;5(1):1–16.